High-spin spectroscopy of ^{139}Ce

S. Kaim,[1,2] C. M. Petrache,[1] A. Gargano,[3] N. Itaco,[3] T. Zerrouki,[1] R. Leguillon,[1,*] A. Astier,[1] I. Deloncle,[1] T. Konstantinopoulos,[1] J. M. Régis,[4] D. Wilmsen,[4] B. Melon,[5] A. Nannini,[5] C. Ducoin,[6] D. Guinet,[6] and T. Bhattacharjee[7]

[1]*Centre de Sciences Nucléaires et de Sciences de la Matière, Université Paris-Sud and CNRS/IN2P3, 91405 Orsay, France*

[2]*Université de Mentouri Constantine, 25017 Constantine, Algeria*

[3]*Dipartimento di Scienze Fisiche, Universitá di Napoli Federico II, and Istituto Nazionale di Fisica Nucleare, Complesso Universitario di Monte S. Angelo, Via Cintia, I-80126 Napoli, Italy*

[4]*Institut für Kernphysik der Universität zu Köln, 50937 Köln, Germany*

[5]*Department of Physics and INFN Sezione di Firenze, Firenze, Italy*

[6]*IPNL CNRS/IN2P3 and Université Lyon 1, 69622 Villeurbanne, France*

[7]*Variable Energy Cyclotron Centre, Kolkata 700064, India*

(Received 21 October 2014; revised manuscript received 28 January 2015; published 20 February 2015)

High-spin states in ^{139}Ce have been populated using the ^{130}Te(^{14}C,5n) reaction. The level scheme has been extended to higher spins, including a new band of dipole transitions. The parity of several states has been changed from negative to positive, mainly based on the comparison with the level structure of the core nucleus ^{140}Ce and the results of a realistic shell-model calculation. The dipole band is interpreted as a magnetic rotation band with $\pi h_{11/2}^2 \otimes \nu h_{11/2}^{-1}$ configuration built on small deformation axial shape with ($\varepsilon_2 = 0.12, \gamma = 0^\circ$).

DOI: 10.1103/PhysRevC.91.024318 PACS number(s): 21.10.Re, 21.60.Ev, 23.20.Lv, 27.60.+j

I. INTRODUCTION

The nuclei with $A \sim 140$ having a few holes in the $N = 82$ shell closure are spherical or only slightly deformed in the ground state and at small angular momenta [1], but can get deformed at high spins under the stress of aligned particles, as evidenced by recent experimental results in the $^{138-141}$Nd nuclei [2–6]. The Ce isotopes with neutron number close to $N = 82$ are more difficult to populate at high spins due to the lack of proper projectile-target combinations. However, the investigation of these nuclei is very important for the test of the effective interactions used in shell-model calculations and the existence of dipole bands showing magnetic rotation. New experimental data have been recently published for the ^{137,138}Ce nuclei [7,8] revealing the existence of dipole bands at the highest spins. Results on the ^{139}Ce nucleus were also published recently, but not at high enough spin to possibly observe dipole bands or other collective structures [7–10].

We have studied the ^{139}Ce nucleus by means of the ^{130}Te(^{14}C,5n) reaction, with the main motivation to search for high-spin bands similar to those recently identified in ^{141}Nd [6]. We have observed several new transitions between the previously reported low- and medium-spin states and one band consisting of dipole transitions at high spins. We have also extended the level scheme up to $I^\pi = 43/2^-$ and $E_x = 7988$ keV.

The structure of the observed low- and medium-spin states is investigated using realistic shell-model calculations, while the configuration of the dipole band is assigned on the basis of cranked Nilsson-Strutinsky (CNS) [11–13] and tilted axis cranking (TAC) [14–16] calculations.

The details of the experimental setup are presented in Sec. II. The results of the data analysis are presented in Sec. III and discussed within the framework of shell-model and TAC calculations in Sec. IV. Finally, the summary is given in Sec. V.

II. EXPERIMENTAL DETAILS

High-spin states in ^{139}Ce have been populated in the ^{130}Te(^{14}C,5n) reaction employing an 82 MeV ^{14}C beam delivered by the Tandem accelerator of IPN Orsay. The beam energy of 82 MeV, optimal for the population of the 5n reaction channel, was chosen performing a three-point excitation function at 80, 85, and 90 MeV. The ^{130}Te target with a thickness of 2 mg/cm^2 was deposited on a 120 mg/cm^2 Bi backing and 136 mg/cm^2 copper for heat dissipation. The γ-ray coincidences were measured with the ORGAM array consisting of 13 coaxial Ge detectors with BGO Compton-suppression shields. The Ge detectors were positioned at five different angles with respect to the beam axis: one at 47°, two at 86°, four at 94°, two at 133°, and four at 157°.

The 5n reaction channel leading to ^{139}Ce was populated with a cross sections of around 0.9 b as calculated with PACE4 [17]. The recoiling residual nuclei were stopped by the thick Bi backing in the center of the array. In addition to prompt γ-ray measurements, delayed γ rays from isomeric decays were also measured. For this purpose, a beam pulsing was realized using a chopper-buncher system which produced Gaussian beam pulses with FWHM of 1.8 ns and full width at tenth maximum (FWTM) of 5 ns. A repetition rate of 200 ns was chosen between the beam pulses in order to be able to measure the lifetime of possible new isomeric states. We have measured single γ rays and their detection time with respect to the beam pulse to deduce the lifetime of the isomeric states. However, no new isomeric states in ^{139}Ce have been identified from the present data.

*Present address: Advanced Science Research Center, Japan Atomic Energy Agency, 2-4 Shirakata Shirane, Tokai, Ibaraki 319-1195 Japan.

Events were written on disk employing the NARVAL program [18]. The data were collected using the Orsay acquisition system based on COMET-6X cards [19], designed to be used as high-resolution ADCs. The recorded γ-coincidence events were sorted in various two- and three-dimensional arrays with a wide time gate of 160 ns. We collected 7.6×10^9 γ events from which we could extract 6×10^7 γ-γ and 11×10^6 γ-γ-γ coincidence events. The analysis was performed with the RADWARE [20,21] programs.

To determine the multipolarity of transitions, we used two methods: the directional correlation of oriented states ratios ($R_{\rm DCO}$) and the anisotropy ratios (R_θ). The DCO ratios $R_{\rm DCO}$ were extracted from an asymmetric γ-γ coincidence matrix with the detectors at 84° and 96° on one axis and the detectors at 47° and 133° on the other axis. The anisotropy ratios R_θ have been deduced from two matrices sorted with all detectors on one axis, and the detectors at (86°, 94°) and at forward/backward (f,b) angles, respectively, on the other axis. Gates were set on the axis with all detectors, and the intensity ratio $R_\theta = W(\text{f,b})/W(86^\circ,94^\circ)$ was determined for the transitions in the resulting spectra. The multipolarities of the new transitions identified in ^{139}Ce were assigned based on the comparison of the deduced DCO and anisotropy ratios with the average ratios extracted for known pure $E2$ and $M1/E1$ transitions in the strongly populated ^{138}Ce nucleus. The DCO ratios for pure quadrupole and dipole transitions are 1.0 and 0.6, respectively, when gating on a pure quadrupole transition, and 2.0 and 1.0 when gating on a pure dipole transition. The anisotropy ratios for pure quadrupole and dipole transitions were 1.02 and 0.7, respectively, independent of the gating transition. The present measurement did not allow to distinguish between electric and magnetic transitions. Therefore, the parities assigned to the positive-parity states are only based on the comparison with the shell model calculations presented in Sec. VI.

III. RESULTS AND LEVEL SCHEME

The information obtained from the present experiment about the observed transitions is given in Table I.

The level scheme of ^{139}Ce is shown in Fig. 1. Spectra obtained by gating on selected transitions of the different band structures are shown in Fig. 2.

The large majority of the previously observed states up to spin $31/2^-$ [9,10] are confirmed, excepting some tentative transitions reported in Ref. [10]. We identified 29 new transitions. Two of them with energies of 197 and 1409 keV were placed parallel to the 1607 keV transition populating the $11/2^-$ isomer, establishing a new state with spin $(13/2^-)$ at 2164 keV. We have also observed a transition of 1244 keV populating the $23/2^-$ state at 3187 keV.

The remaining 26 new transitions de-excite high-spin states above $I^\pi = 31/2^-$ and $E_x = 4808$ keV. One of the important changes with respect to the level scheme reported in Ref. [10] is that the $33/2^-$ state at 5917.3 and the $31/2^-$ state at 5916.3 keV are merged in a single $33/2^-$ state at 5916.5 keV. This was possible based on the following arguments. (i) The 239 keV transition, as well as transitions of band D1 above the level at 5917 keV, are in coincidence with the cascades populated by the 384 keV and the 1108 keV transitions. (ii) The $R_{\rm DCO}$ ratio of the 404 keV transition when gated on an $M1$ transition comes out to be 2.02(30) in the present work, which is therefore compatible with a $\Delta I = 2$ transition, leading to spin $31/2^-$ for the state at 4808 keV. (iii) The $R_{\rm DCO}$ ratio of the 1108 keV transition comes out to be 0.35(8) in the present work when gated on an $E2$ transition, which is compatible with a $M1 + E2$ transition, leading thus to spin $33/2^-$ for the state at 5916.5 keV.

Another important difference with respect to the previous published level schemes [9,10] is that we assign positive parity to the cascades built on top of the $23/2^+$ and $25/2^+$ states, which in turn decay via the 1194, 897, and 206 keV transitions to the negative-parity states built on top of the $19/2^-$ isomer. This assumption is based on the comparison with the level structure of the core nucleus ^{140}Ce [22,23], which presents strongly populated low-lying negative-parity states based on $h^1_{11/2}(d_{5/2}/g_{7/2})^1$ proton configurations. The coupling of one neutron hole in the $h_{11/2}$ orbital with the negative-parity states of ^{140}Ce are therefore expected to lead to positive-parity states with medium spins in ^{139}Ce nucleus, which are in fact predicted by shell-model calculations (see the discussion in Sec. IV A).

At high spins we observed several weakly populated states up to spin $43/2^-$ and excitation energy of 8 MeV. Two cascades of dipole transitions have been identified: one consisting of the 176, 466, 511, and 548 keV transitions on top of the $35/2^-$ state at 6155 keV, and one consisting of the 219, 226, 346, 357, 488, and 654 keV transitions on top of the $31/2^-$ state at 5916.5 keV, which we label D1 and will be discussed in the following section.

IV. DISCUSSION

As mentioned in the Introduction, we have performed shell-model as well as TAC calculations to interpret the structure of the levels of ^{139}Ce observed in the present experiment. More precisely in Sec. IV A we present the results of a realistic shell-model calculation by limiting to states with low and medium spin. The D1 band is discussed in Sec. IV B in terms of the TAC calculations.

A. Shell-model calculations

In our calculations we assume ^{132}Sn as closed core and let the valence particles, namely, eight protons and one neutron hole, occupy the five orbits $1g_{7/2}$, $2d_{5/2}$, $1h_{11/2}$, $2d_{3/2}$, $3s_{1/2}$ of the 50–82 shell. The adopted Hamiltonian is the same we employed in our recent shell-model studies of nuclei around ^{132}Sn [24,25]. In particular, the proton single-particle energies, relative to the $1g_{7/2}$ level, are (in MeV): $\epsilon_{2d_{5/2}} = 0.962$, $\epsilon_{2d_{3/2}} = 2.439$, $\epsilon_{1h_{11/2}} = 2.793$, $\epsilon_{3s_{1/2}} = 2.800$, while the neutron single-hole energies, relative to the $2d_{3/2}$ orbit: $\epsilon^{-1}_{1h_{11/2}} = 0.069$, $\epsilon^{-1}_{3s_{1/2}} = 0.332$, $\epsilon^{-1}_{1d_{5/2}} = 1.654$, $\epsilon^{-1}_{1g_{7/2}} = 2.434$. These values are taken from the experimental spectra of ^{133}Sb and ^{131}Sn [26], respectively, the only exception being that of the $3s_{1/2}$ proton orbit, which is still missing in the observed spectrum of ^{133}Sb. The position of this orbit, as discussed in [27], has been determined by reproducing the experimental energy of the $1/2^+$ state at 2.150 MeV in ^{137}Cs [28]. Note that the energy

TABLE I. Energies, intensities, anisotropies, DCO ratios, multipolarities, and spin-parity assignments of γ-ray transitions of ^{139}Ce obtained from the present experiment. The new transitions, new levels, and new spin-parity assignments are indicated with bold fonts, while modified spin-parity assignments are indicated with italic fonts.

E_γ (keV)[a]	I_γ[b]	E_i (keV)	R_θ[c]	R_θ[d]	$R_{\rm DCO}$[c]	$R_{\rm DCO}$[d]	Multipolarity	$J_i^\pi \rightarrow J_f^\pi$
61.0	1.0	5884.5						**35/2$^-$** $\rightarrow$ **(33/2$^-$)**
70.1	6.4	4083.5						*25/2$^+$* $\rightarrow$ *23/2$^+$*
166.0	3.7	**5698.9**						**31/2$^-$** $\rightarrow$ **31/2$^+$**
176.4	2.7	**6331.8**		1.19(19)	0.86(30)	1.24(20)	$M1+E2$	**37/2$^-$** $\rightarrow$ **35/2$^-$**
187.8	82.9	2819.8		1.33(32)	0.76(12)	1.15(14)	M1+E2	21/2$^-$ $\rightarrow$ 19/2$^-$
192.8	5.6	**6077.2**						**(35/2$^-$)** $\rightarrow$ **35/2$^-$**
193.2	27.0	4276.7		1.38(12)	0.74(4)	1.53(1)	$M1+E2$	*27/2$^+$* $\rightarrow$ *25/2$^+$*
197.0	4.5	2361.4						**15/2$^-$** $\rightarrow$ **(13/2$^-$)**
206.4	3.7	4083.5						*25/2$^+$* $\rightarrow$ *23/2$^-$*
218.6	3.3	5916.5	0.63(30)		0.42(20)	1.30(70)	$M1+E2$	**33/2$^-$** $\rightarrow$ **31/2$^-$**
221.7	3.5	4100.1						25/2$^-$ $\rightarrow$ 23/2$^-$
226.0	6	**6142.6**		1.11(18)	0.53(16)	1.46(8)	$M1+E2$	**35/2$^-$** $\rightarrow$ **33/2$^-$**
234.7	3	5533.2	1.08(30)	1.09(30)	0.62(05)	1.10(16)	$M1+E2$	*31/2$^+$* $\rightarrow$ *29/2$^+$*
239.0	6.1	6155.5		1.07(17)	0.61(7)	1.23(30)	$M1+E2$	35/2$^-$ $\rightarrow$ 33/2$^-$
253.0	0.8	**6331.8**						**37/2$^-$** $\rightarrow$ **(35/2$^-$)**
270.6	100.0	2632.0		1.39(30)	0.86(20)	1.68(4)	$E2$	19/2$^-$ $\rightarrow$ 15/2$^-$
293.7	5.8	**6032.4**	0.84(14)	1.02(10)	0.54(20)	1.01(20)	$M1+E2$	**33/2$^+$** $\rightarrow$ **31/2$^+$**
298.3	6.7	2361.4				1.52(18)	$M1+E2$	15/2$^-$ $\rightarrow$ (11/2$^-$,13/2$^-$)
305.5	25.3	4404.5	0.81(19)	0.90(16)	0.51(11)	1.10(30)	$M1+E2$	27/2$^-$ $\rightarrow$ 25/2$^-$
345.8	5.2	**6488.5**	0.75(12)		0.44(5)	0.89(10)	$M1+E2$	**37/2$^-$** $\rightarrow$ **35/2$^-$**
356.6	4.5	**6845.3**		0.68(30)			$M1+E2$	**39/2$^-$** $\rightarrow$ **37/2$^-$**
367.2	57.8	3187.0	0.74(30)		0.47(17)		$M1+E2$	23/2$^-$ $\rightarrow$ 21/2$^-$
383.4	7.8	5916.5		0.74(12)	0.40(3)	1.05(40)	$E1$	*33/2$^-$* $\rightarrow$ *31/2$^+$*
403.9	29.9	4808.4		1.21(40)		2.02(30)	$E2$	*31/2$^-$* $\rightarrow$ *27/2$^-$*
439.1	3.5	**5737.5**				1.01(16)	$M1+E2$	**31/2$^+$** $\rightarrow$ **29/2$^+$**
447.4	5.5	**6331.8**		0.71(30)			$M1+E2$	**37/2$^-$** $\rightarrow$ **35/2$^-$**
465.5	1.2	**6797.5**		0.44(13)			$M1+E2$	**39/2$^-$** $\rightarrow$ **37/2$^-$**
479.8	15.5	4756.6		0.72(9)	0.41(14)	0.94(19)	$M1+E2$	*29/2$^+$* $\rightarrow$ *27/2$^+$*
488.3	5.8	**7333.6**		0.28(17)			$M1+E2$	**41/2$^-$** $\rightarrow$ **39/2$^-$**
510.9	3.0	**7309.5**						**(41/2$^-$)** $\rightarrow$ **39/2$^-$**
547.5	2.2	**7856.9**						**(43/2$^-$)** $\rightarrow$ **(41/2$^-$)**
642.7	3.0	**6797.5**						**39/2$^-$** $\rightarrow$ **35/2$^-$**
654.3	4.3	**7987.6**		0.52(15)		0.95(30)	$M1+E2$	**43/2$^-$** $\rightarrow$ **41/2$^-$**
776.1	5.3	5532.5		0.58(12)	0.52(11)		$M1+E2$	*31/2$^+$* $\rightarrow$ *29/2$^+$*
835.9	3.6	**8001.1**						
889.8	3.1	**6967.0**						$\rightarrow$ **(35/2$^-$)**
896.5	28.1	4083.5			0.49(17)	0.91(14)	$E1$	**25/2$^+$** $\rightarrow$ **23/2$^-$**
911.6	6.0	4100.1			0.54(14)		$M1+E2$	25/2$^-$ $\rightarrow$ 23/2$^-$
1013.6	3.7	**5822.0**						**(33/2$^-$)** $\rightarrow$ **31/2$^-$**
1021.6	4.2	5298.9	0.25(11)	0.35(11)			$M1+E2$	*29/2$^+$* $\rightarrow$ *27/2$^+$*
1057.7	8.0	3877.4	0.35(17)				$M1+E2$	23/2$^-$ $\rightarrow$ 21/2$^-$
1076.0	12.7	5884.5	1.07(17)			1.60(40)	$E2$	*35/2$^-$* $\rightarrow$ *31/2$^-$*
1088.0	3.6	**7165.2**						$\rightarrow$ **(35/2$^-$)**
1108.1	10.6	5916.5	0.60(20)	0.66(7)	0.35(8)		$M1+E2$	*33/2$^-$* $\rightarrow$ *31/2$^-$*
1118.0	0.2	**7450.0**						$\rightarrow$ **37/2$^-$**
1160.1	1.5	5916.5						*33/2$^-$* $\rightarrow$ *29/2$^+$*
1194.3	10.1	4014.3	0.56(16)	0.72(41)			$E1$	*23/2$^+$* $\rightarrow$ *21/2$^-$*
1214.4	3.1	5299.9						*29/2$^+$* $\rightarrow$ *25/2$^+$*
1217.5	11.6	4404.5			1.02(7)	1.84(30)	$E2$	27/2$^-$ $\rightarrow$ 23/2$^-$
1240.0	0.3	**7571.6**						$\rightarrow$ **37/2$^-$**
1244.4	7.1	**4431.5**						$\rightarrow$ **23/2$^-$**
1256.5	5.5	5533.2			0.99(40)		$E2$	*31/2$^+$* $\rightarrow$ *27/2$^+$*
1280.3	15.1	4100.1	0.95(50)		0.94(30)		$E2$	25/2$^-$ $\rightarrow$ 21/2$^-$
1293.3	2.1	**5698.9**						**31/2$^-$** $\rightarrow$ **27/2$^-$**
1310.2	6.8	2064.1						(11/2$^-$,13/2$^-$) $\rightarrow$ 11/2$^-$
1409.4	5.5	**2164.4**				1.59(60)	$(M1+E2)$	**(13/2$^-$)** $\rightarrow$ **11/2$^-$**

TABLE I. (*Continued.*)

E_γ (keV)[a]	I_γ[b]	E_i (keV)	R_θ[c]	R_θ[d]	$R_{\rm DCO}$[c]	$R_{\rm DCO}$[d]	Multipolarity	$J_i^\pi \rightarrow J_f^\pi$
1460.6	3.5	**5737.5**	1.44(12)	1.27(40)		1.62(19)	$E2$	$\mathbf{31/2^+ \rightarrow 27/2^+}$
1607.2	95.8	2361.4		1.33(30)		1.87(50)	$E2$	$15/2^- \rightarrow 11/2^-$

[a]The error on the transition energies is 0.2 keV for transitions below 1000 keV and intensities larger than 5% of the ^{139}Ce reaction channel, 0.5 keV for transitions above 1000 keV and intensities lower than 5%, and 1 keV for transitions above 1200 keV and/or weaker than 1%.
[b]Relative intensities corrected for efficiency. The transition intensities were obtained from a combination of total projection and gated spectra.
[c]Gate on the 1607 keV $E2$ transition.
[d]Gate on the 188 keV $M1$ transition.

of the $h_{11/2}$ neutron orbit corresponds to the value measured in Ref. [29].

As for the two-body component of the effective Hamiltonian, we employ a realistic effective interaction derived from the CD-Bonn nucleon-nucleon potential [30] renormalized following the $V_{\rm low\text{-}k}$ approach [31] with a cutoff momentum $\Lambda = 2.2\,{\rm fm}^{-1}$. The obtained low-momentum potential plus the Coulomb force for protons is then used to derive the two-body effective interaction $V_{\rm eff}$ within the framework of the $\hat{Q}$-box folded diagram expansion [32], including diagrams up to second order in the interaction. These diagrams are computed within the harmonic-oscillator basis using intermediate states composed of all possible hole states and particle states restricted to the five proton and neutron shells above the Fermi

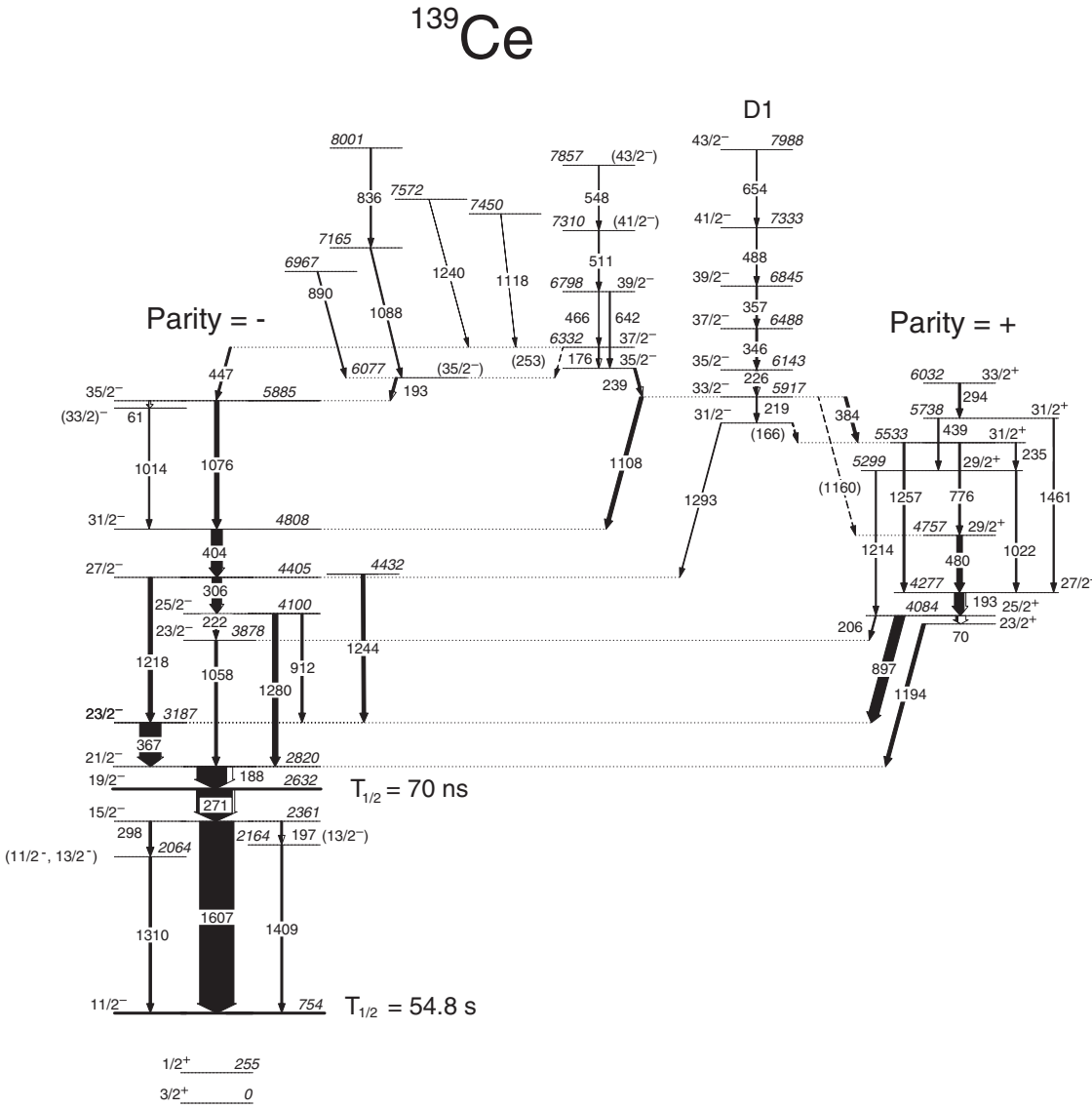

FIG. 1. Level scheme of ^{139}Ce. Band D1 and the levels above the cascades of positive and negative parity are new.

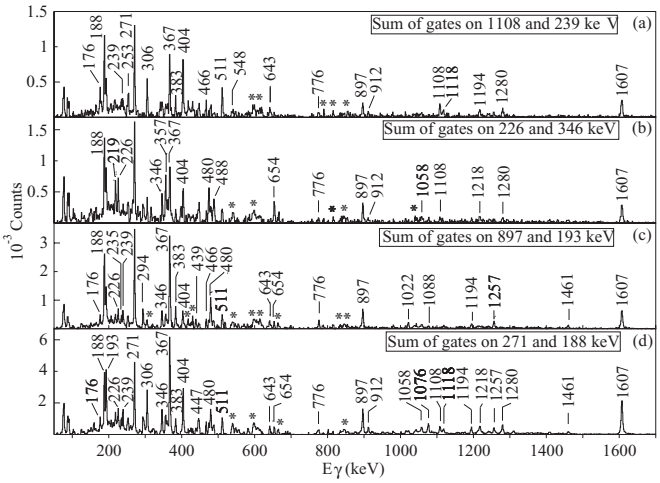

FIG. 2. Spectra of the various structures identified in ^{139}Ce. (a) Sum of the spectra with gates on the 1108 and 239 keV transitions showing the high-spin states; (b) sum of the spectra with gated on the 226 and 346 keV transitions showing the band D1; (c) sum of the spectra with gates on the 897 and 193 keV transitions showing the states grouped in the cascades "Parity = +"; (d) sum of the spectra with gates on 271 and 188 keV transitions showing the states grouped in the cascades "Parity = −". The transitions marked with an asterisk belong to ^{138}Ce.

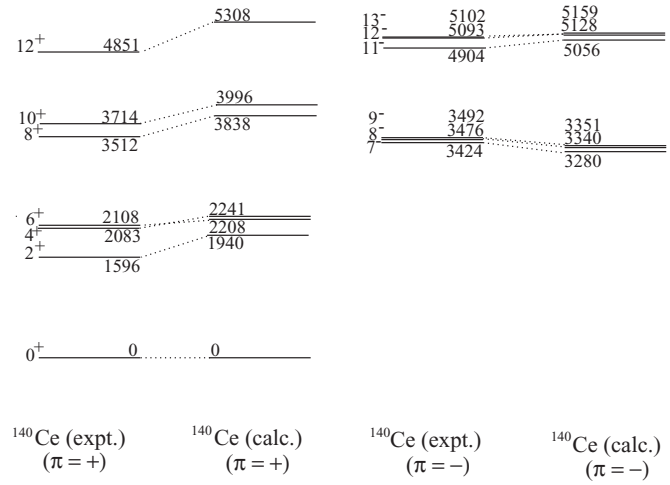

FIG. 3. Comparison between experimental and calculated levels in ^{140}Ce.

surface. The oscillator parameter is 7.88 MeV as obtained from the expression $\hbar\omega = 45A^{-1/3} - 25A^{-2/3}$ with $A = 132$. It is worth mentioning that the proton-neutron effective interaction has been derived in the particle-hole representation, while the proton-proton one in the usual particle-particle representation. The shell model calculations have been performed with the OSLO code [33].

As a first step, we have calculated the spectroscopic properties of the $N = 82$ ^{140}Ce isotope. This allows to test separately the proton component of the interaction and may give us the framework to understand our results for ^{139}Ce in terms of a neutron hole coupled to ^{140}Ce by looking at the effects of the neutron-proton interaction. The comparison of the experimental [26] and calculated spectra of ^{140}Ce is given in Fig. 3. One can see that the energies of the negative-parity levels are very well reproduced by the theory, the discrepancy ranging from about 30 to 150 keV. The quality of the agreement is not so good for the positive-parity states: the 4^+ and 6^+ states are well reproduced, while the experimental energies of the other positive-parity states are overestimated by about 300 keV and more. It is worth mentioning the recent work by Srivastava *et al.* [34], where some $N = 82$ isotones, including ^{140}Ce, were studied within the shell model by considering the same model space used in our calculation but starting from the doubly magic ^{100}Sn core. In [34] all the calculated levels for ^{140}Ce are predicted to lie below the experimental ones and, at variance with our results, a better agreement is obtained for the positive-parity states.

Let us now come to discuss ^{139}Ce. In Fig. 4 the experimental spectrum observed in the present work is compared with the calculated one, both spectra being referred to the $11/2^-$ excited state. Note that we do not include states with $J > 33/2$, located in the higher-energy region above 5.9 MeV, since their description is likely to require configurations outside the chosen model space.

First, we see that our calculation reproduces the structure of the experimental spectrum, which is characterized by three groups of negative-parity levels well separated in energy lying above the $11/2^-$ state, and by two groups of positive-parity levels with the $29/2^+$ state in between them. From a quantitative point of view, a very good agreement between theory and experiment is obtained for the excitation energies of the positive-parity states. This is not the case, however, for the negative-parity states, which are all overestimated within a range going from less than 100 to about 500 keV. Aside from these uncertainties, the quality of the agreement is such as to allow us to identify the observed $(13/2^-, 11/2^-)$ level at 1.310 MeV with our calculated $11/2^-$ state at 1.757 MeV.

It is worth noting that, exchanging the parity of states, the level scheme for ^{139}Ce follows that of ^{140}Ce shown in Fig. 3, as evidenced in Fig. 5 where the experimental spectra of these two nuclei are compared. This may be explained by interpreting each group of levels of ^{139}Ce as arising essentially

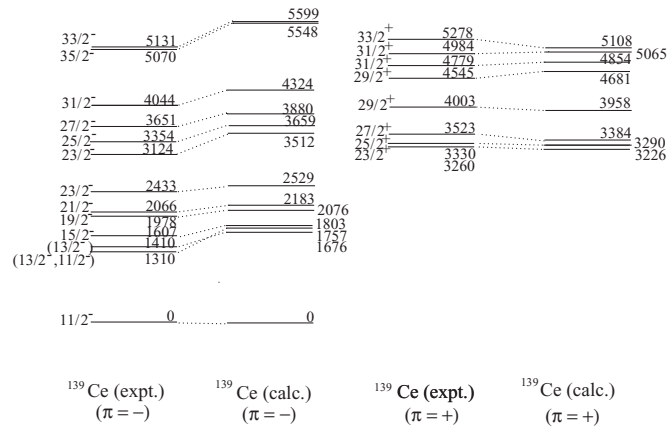

FIG. 4. Comparison between experimental and calculated levels in ^{139}Ce.

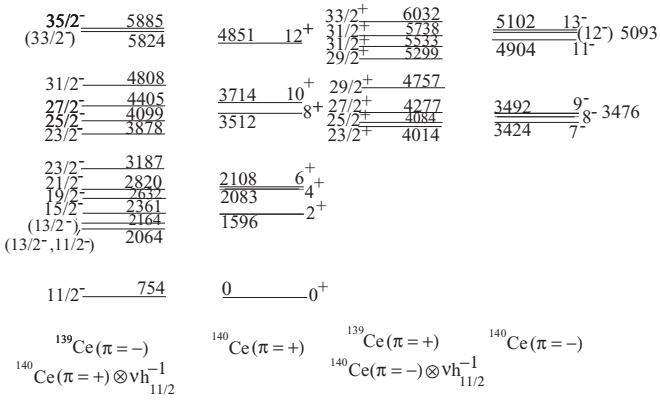

FIG. 5. Comparison between the experimental levels in ^{139}Ce and in the core nucleus ^{140}Ce.

from the coupling of a neutron hole in the $h_{11/2}$ orbit to the group of ^{140}Ce in the same energy range. In fact, from our calculation it turns out that all the states of ^{139}Ce are characterized by a vacancy in the $h_{11/2}$ orbit equal to about 1, while corresponding groups of levels in ^{139}Ce and ^{140}Ce show a distribution of protons on the single-particle orbits with similar features. However, when going from ^{140}Ce to ^{139}Ce one has to consider the effects of the neutron-proton interaction that give rise to a rearrangement of the protons. In particular, we find that the very small occupancy of the $d_{3/2}$ and $s_{1/2}$ orbits, only 1–5 % of protons are in these two orbits, remains unchanged, while the number of protons in the $g_{7/2}$ orbit decreases in favor essentially of the $d_{5/2}$ orbit. This is related to the fact that the matrix elements of our proton-neutron effective interaction, which is written in the particle-hole channel, are overall more repulsive for the $\pi h_{11/2}^{-1} \otimes \nu g_{7/2}$ configuration than for the $\pi h_{11/2}^{-1} \otimes \nu d_{5/2}$ configuration.

In order to get confidence in the interpretation of the observed states, we have also calculated the transition probabilities for the excited levels of ^{139}Ce, using the following parameters: $e_{eff}^{p} = 1.7e, e_{eff}^{n} = 0.7e, g_l^p = 1, g_l^n = 0, g_s^p = 0.7$, $g_s^{\text{free}} = 3.91, g_s^n = 0.7$, $g_s^{\text{free}} = -2.47$ [24].

The value of $B(E2; 19/2^- \rightarrow 15/2^-)$ deduced from the $T_{1/2} = 70$ ns of the $19/2^-$ state [26] is 8.19 e^2fm^4, which is in the same range as the calculated value of 2.25 e^2fm^4. The results for the branching ratios are summarized in Table II. One can see that the calculated branching ratios reproduce the experimental variation for the different states, being in better agreement for the negative-parity states. Most of the $\Delta I = 1$ transitions are predicted to have a mixed $M1/E2$ character.

B. The $\Delta I = 1$ band interpreted by TAC calculations

The configuration of the dipole band in ^{139}Ce can be understood within the tilted axis cranking (TAC) model [14–16], through calculations similar to those recently performed for the dipole bands in ^{138}Nd [35]. The lowest-lying configurations involve two $h_{11/2}$ protons which align their angular momenta with the short axis, because this orientation corresponds to maximal overlap of their doughnut-like density distribution with the triaxial core. As a consequence, the $h_{11/2}$ protons favor rotation about the short axis. As seen in the middle panels of Fig. 7 of Ref. [35], the single-particle proton Routhians A and B have a pronounced minimum at $\theta = 90^\circ$. The neutron configuration at high spins would involve one neutron hole in the $h_{11/2}$ orbital, with the angular momentum aligned along the long axis, because this orientation minimizes the overlap with the triaxial core. As a consequence, the $h_{11/2}$ neutron hole favors the rotation about the long axis. As seen in the middle panel of Fig. 8 of Ref. [35], the single-particle neutron Routhians $\bar{A}$ has a pronounced maximum at $\theta = 0^\circ$, which means that a hole in this orbital drives the rotational axis to $\theta = 0^\circ$. Alternatively one may say that the neutron on A favors the long axis. The $h_{11/2}$ neutrons on the lower orbitals do not drive the rotational axis significantly, because to each single-particle Routhian there is a conjugate one (barred) that nearly compensates the drive.

The TAC calculations were performed for the various negative-parity configurations assuming the deformations calculated with the CNS model [11–13]. We investigated the lowest-lying configurations involving one, two, or three protons in $h_{11/2}$ coupled with one neutron in $h_{11/2}$. The quadrupole

TABLE II. Experimental and calculated branching ratios for excited levels of ^{139}Ce.

Branching ratios	$\frac{E_\gamma(\Delta I=1)(\text{keV})}{E_\gamma(E2)(\text{keV})}$	Exp. $\frac{B(\Delta I=1)}{B(E2)(\mu_n^2/(\text{eb})^2)}$	Calc. $\frac{B(M1)}{B(E2)(\mu_n^2/(\text{eb})^2)}$	Calc. $\frac{B(E2,\Delta I=1)}{B(E2)}$
$\frac{15/2^-\rightarrow 13/2^-}{15/2^-\rightarrow 11/2^-}$	$\frac{197}{1607}$	46(10)	21	0.48
$\frac{25/2^-\rightarrow 23/2_2^-}{25/2^-\rightarrow 21/2^-}$	$\frac{222}{1280}$	940(180)	84	0.67
$\frac{25/2^-\rightarrow 23/2_1^-}{25/2^-\rightarrow 21/2^-}$	$\frac{912}{1280}$	8(2)	0.1	0.015
$\frac{27/2^-\rightarrow 25/2^-}{27/2^-\rightarrow 23/2_1^-}$	$\frac{306}{1218}$	140(45)	240	23
$\frac{29/2_2^+\rightarrow 27/2^+}{29/2_2^+\rightarrow 25/2^+}$	$\frac{1022}{1214}$	2.3(6)	0.4	0.042
$\frac{31/2_1^+\rightarrow 29/2_1^+}{31/2_1^+\rightarrow 27/2^+}$	$\frac{776}{1257}$	4.5(9)	0.5	0.0060
$\frac{31/2_1^+\rightarrow 29/2_2^+}{31/2_1^+\rightarrow 27/2^+}$	$\frac{235}{1257}$	91(19)	210	3.62
$\frac{31/2_2^+\rightarrow 29/2_2^+}{31/2_2^+\rightarrow 27/2^+}$	$\frac{439}{1461}$	39(9)	2.3	0.153

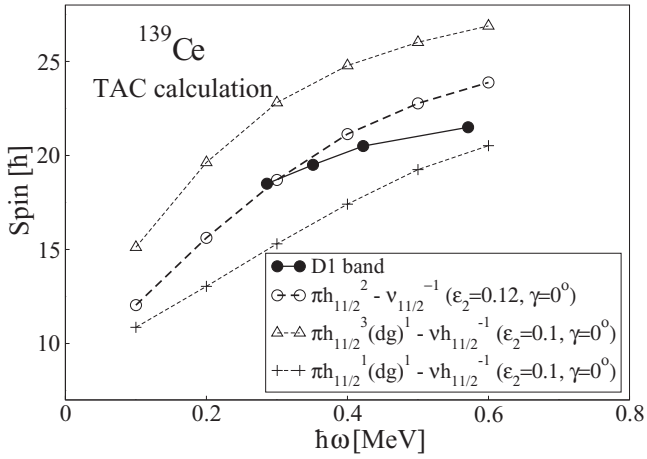

FIG. 6. TAC calculations for the band D1 of ^{139}Ce. Filled (open) symbols are used for the experimental (calculated) band. The lines linking the points are used to guide the eyes. The deformation parameters for each configuration are those calculated with the CNS model. The configurations are given in terms of unpaired proton particles and neutron holes.

deformations of these configurations are small ($\varepsilon_2 \approx 0.1$) and the shape is nearly axial ($\gamma \approx 0^\circ$). The calculated bands are shown in Fig. 6. One can see that one obtains calculated aligned spins close to the experimental values for the configuration $\pi h^2_{11/2} \otimes \nu h^{-1}_{11/2}$. The calculated tilted angle is $\theta \approx 70^\circ$. The less satisfactory agreement for the highest observed spins can be due to a gradual shape change as recently observed in the ^{141}Nd isotope [6]. The calculated B(M1) values decrease with increasing rotation frequency from 5 μ_n^2 for $\hbar\omega = 0.1$ to 3 μ_n^2 for $\hbar\omega = 0.6$, indicating the presence of the shears-bands mechanism [36].

V. SUMMARY

High-spin states in ^{139}Ce have been populated using the ^{130}Te(^{14}C,5n) reaction. The level scheme has been extended to higher spins, including a new dipole band. The parity of several states has been changed from negative to positive, mainly based on the comparison with the level structure of the core nucleus ^{140}Ce. Extended shell-model calculations have been used to investigate the structure of the observed states. The good agreement of the shell-model calculations with the experimental level scheme supports the spin-parity assignment to low- and medium-spin states. The dipole band configuration was investigated using the CNS and TAC models. The $\pi 1h^2_{11/2} \otimes \nu 1h^{-1}_{11/2}$ configuration with a deformation of ($\varepsilon_2 = 0.12, \gamma = 0^\circ$) and rotation around a tilted axis with $\theta \approx 70^\circ$, best reproduces the experimental aligned spins.

ACKNOWLEDGMENTS

The authors acknowledge the tandem group at IPN Orsay for the help during the experiment and for providing the heavy-ion beam.

[1] P. Möller, J. R. Nix, W. D. Myers, and W. J. Swiatecki, At. Data Nucl. Data Tables **59**, 185 (1995).
[2] C. M. Petrache, I. Ragnarsson, Hai-Liang Ma, R. Leguillon, T. Konstantinopoulos, T. Zerrouki, D. Bazzacco, and S. Lunardi, Phys. Rev. C **88**, 051303(R) (2013).
[3] C. M. Petrache, I. Ragnarsson, Hai-Liang Ma, R. Leguillon, T. Zerrouki, D. Bazzacco, and S. Lunardi, Phys. Rev. C **91**, 024302 (2015).
[4] S. Bhowal, G. Gangopadhyay, C. M. Petrache, I. Ragnarsson, A. K. Singh, S. Bhattacharya, H. Hübel, A. Neußer-Neffgen, A. Al-Khatib, P. Bringel, A. Bürger, N. Nenoff, G. Schönwasser, G. B. Hagemann, B. Herskind, D. R. Jensen, G. Sletten, P. Fallon, A. Görgen, P. Bednarczyk, D. Curien, A. Korichi, A. Lopez-Martens, B. V. T. Rao, T. S. Reddy, and Nirmal Singh, Phys. Rev. C **84**, 024313 (2011).
[5] R. Leguillon, C. M. Petrache, T. Zerrouki, T. Konstantinopoulos, K. Hauschild, A. Korichi, A. Lopez-Martens, S. Frauendorf, I. Ragnarsson, P. T. Greenlees, U. Jakobsson, P. Jones, R. Julin, S. Juutinen, S. Ketelhut, M. Leino, P. Nieminen, M. Nyman, P. Peura, P. Rahkila, P. Ruotsalainen, M. Sandzelius, J. Saren, C. Scholey, J. Sorri, J. Uusitalo, H. Hübel, A. Neußer-Neffgen, A. Al-Khatib, A. Bürger, N. Nenoff, A. K. Singh, D. Curien, G. B. Hagemann, B. Herskind, G. Sletten, P. Fallon, A. Görgen, P. Bednarczyk, and D. M. Cullen, Phys. Rev. C **88**, 014323 (2013).
[6] T. Zerrouki, C. M. Petrache, R. Leguillon, K. Hauschild, A. Korichi, A. Lopez-Martens, S. Frauendorf, I. Ragnarsson, H. Hübel, A. Neußer-Neffgen, A. Al-Khatib, P. Bringel, A. Bürger, N. Nenoff, G. Schönwasser, A. K. Singh, D. Curien, G. B. Hagemann, B. Herskind, G. Sletten, P. Fallon, A. Görgen, and P. Bednarczyk, Eur. Phys. J. A (to be published).
[7] T. Bhattacharjee, S. Chanda, A. Mukherjee, S. Bhattacharyya, S. Kumar Basu, S. S. Ghugre, U. D. Pramanik, R. P. Singh, S. Muralithar, N. Madhavan, J. J. Das, and R. K. Bhowmik, Phys. Rev. C **78**, 024304 (2008).
[8] T. Bhattacharjee, S. Chanda, S. Bhattacharyya, S. K. Basu, R. K. Bhowmik, J. J. Das, U. Datta Pramanik, S. S. Ghugre, N. Madhavan, A. Mukherjee, G. Mukherjee, S. Muralithar, and R. P. Singh, Nucl. Phys. A **825**, 16 (2009).
[9] D. Bucurescu, G. Cata-Danil, I. Cata-Danil, M. Ivascu, N. Marginean, R. Marginean, L. C. Mihailescu, C. Rusu, and G. Suliman, Eur. Phys. J. A **27**, 301 (2006).
[10] S. Chanda, T. Bhattacharjee, S. Bhattacharyya, A. Mukherjee, S. K. Basu, I. Ragnarsson, R. K. Bhowmik, S. Muralithar, R. P. Singh, S. S. Ghugre, and U. D. Pramanik, Phys. Rev. C **79**, 054332 (2009).
[11] T. Bengtsson and I. Ragnarsson, Nucl. Phys. A **436**, 14 (1985).
[12] A. V. Afanasjev, D. B. Fossan, G. J. Lane, and I. Ragnarsson, Phys. Rep. **322**, 1 (1999).
[13] B. G. Carlsson and I. Ragnarsson, Phys. Rev. C **74**, 011302(R) (2006).
[14] S. Frauendorf, Rev. Mod. Phys. **73**, 463 (2001).
[15] S. Frauendorf, Nucl. Phys. A **557**, 259 (1993).
[16] S. Frauendorf, Nucl. Phys. A **677**, 115 (2000).
[17] http://lise.nscl.msu.edu/pace4.html.

[18] X. Grave, R. Canedo, J.-F. Clavelin, S. Du, and E. Legay, in *14th IEEE-NPSS Real Time Conference, 2005, Stockholm* (IEEE, Piscataway, NJ, 2005).
[19] http://ipnweb.in2p3.fr/sep/domcomp/microelec.html.
[20] D. C. Radford, Nucl. Instrum. Methods Phys. Res. A **361**, 297 (1995).
[21] D. C. Radford, Nucl. Instrum. Methods Phys. Res. A **361**, 306 (1995).
[22] W. Enghardt, H. U. Jäger, L. Käubler, H. J. Keller, H. Prade, and F. Stary, Z. Phys. A **316**, 245 (1984).
[23] L. Käubler, W. Enghardt, H. Prade, H. F. Stary, P. Carlé, L. O. Norlin, K. G. Rensfelt, and U. Rosengard, Hyperfine Interaction **34**, 381 (1987).
[24] M. Danchev *et al.*, Phys. Rev. C **84**, 061306(R) (2011).
[25] L. Coraggio, A. Covello, A. Gargano, and N. Itaco, Phys. Rev. C **88**, 041304(R) (2013).
[26] http://www.nndc.bnl.gov.
[27] F. Andreozzi, L. Coraggio, A. Covello, A. Gargano, T. T. S. Kuo, and A. Porrino, Phys. Rev. C **56**, R16 (1997).
[28] B. H. Wildenthal, E. Newman, and R. L. Auble, Phys. Rev. C **3**, 1199 (1971).
[29] B. Fogelberg *et al.*, Phys. Rev. C **70**, 034312 (2004).
[30] R. Machleidt, Phys. Rev. C **63**, 024001 (2001).
[31] S. Bogner, T. T. S. Kuo, L. Coraggio, A. Covello, and N. Itaco, Phys. Rev. C **65**, 051301(R) (2002).
[32] L. Coraggio, A. Covello, A. Gargano, N. Itaco, and T. T. S. Kuo, Prog. Part. Nucl. Phys. **62**, 135 (2009), and references therein.
[33] T. Engeland, the OSLO shell-model code 1991–2006 (unpublished).
[34] P. C. Srivastava, M. J. Ermamatov, and Irving O. Morales, J. Nucl. G **40**, 035106 (2013).
[35] C. M. Petrache, S. Frauendorf, M. Matsuzaki, R. Leguillon, T. Zerrouki, S. Lunardi, D. Bazzacco, C. A. Ur, E. Farnea, C. Rossi Alvarez, R. Venturelli, and G. de Angelis, Phys. Rev. C **86**, 044321 (2012).
[36] S. Chmel, S. Frauendorf, and H. Hübel, Phys. Rev. C **75**, 044309 (2007).